Soft Matter

CrossMark
← click for updates

Ultra-low voltage electrowetting using graphite surfaces†

Deborah J. Lomax,[a] Pallav Kant,[b] Aled T. Williams,[a] Hollie V. Patten,[a] Yuqin Zou,[a] Anne Juel[b] and Robert A. W. Dryfe*[a]

The control of wetting behaviour underpins a variety of important applications from lubrication to microdroplet manipulation. Electrowetting is a powerful method to achieve external wetting control, by exploiting the potential-dependence of the liquid contact angle with respect to a solid substrate. Addition of a dielectric film to the surface of the substrate, which insulates the electrode from the liquid thereby suppressing electrolysis, has led to technological advances such as variable focal-length liquid lenses, electronic paper and the actuation of droplets in lab-on-a-chip devices. The presence of the dielectric, however, necessitates the use of large bias voltages (frequently in the 10–100 V range). Here we describe a simple, dielectric-free approach to electrowetting using the basal plane of graphite as the conducting substrate: unprecedented changes in contact angle for ultra-low voltages are seen below the electrolysis threshold (50° with 1 V for a droplet in air, and 100° with 1.5 V for a droplet immersed in hexadecane), which are shown to be reproducible, stable over 100 s of cycles and free of hysteresis. Our results dispel conventional wisdom that reversible, hysteresis-free electrowetting can only be achieved on solid substrates with the use of a dielectric. This work paves the way for the development of a new generation of efficient electrowetting devices using advanced materials such as graphene and monolayer MoS_2.

1. Introduction

Wetting phenomena underpin a number of important technological processes,[1–3] with electrowetting finding applications in diverse fields.[4–8] At present, these applications are normally performed with a dielectric layer between the electrode and solution phase.[4,9–11] Reversible electrowetting requires surfaces that are smooth enough to minimize phenomena such as the pinning of droplets[12] and the hysteresis in contact angle between wetting and de-wetting cycles.[13] The seminal work of Frumkin demonstrated that these conditions could be met for aqueous electrolytes on mercury surfaces, however attempts to extend the approach to solid conductors were unsuccessful.[10] Electrowetting on solids has been achieved through the "electrowetting on a dielectric" (EWOD) configuration, referred to above, albeit at the expense of higher voltages.[4–6] An alternative, ultra-low voltage route to "electrowetting on a conductor" (EWOC) that is based on immiscible electrolyte solutions has been proposed.[11,14,15] The immiscible liquid configuration

has been realized experimentally using a sputtered gold film electrode, which although macroscopically smooth, exhibited strong wetting hysteresis due to its micron-scale roughness. The latter could be overcome through the use of a voltage pulsing technique (to ±2 V) as suggested,[16] and subsequently rationalized.[17] Such contact angle hysteresis is also commonly encountered in the more conventional EWOD configuration: alternating voltage methods have been shown to minimise these effects for electrowetting in liquid/air[18,19] and liquid/liquid configurations,[20] respectively.

Herein we return to the canonical droplet configuration pioneered by Frumkin to demonstrate a robust and versatile approach to reversible and hysteresis-free EWOC, see Fig. 1(a), which does not require the application of an alternating voltage or voltage pulses to overcome hysteresis. Reversible wetting is shown to occur on a laminar conductor, the basal plane of highly oriented pyrolytic graphite (HOPG). HOPG can be readily refreshed by mechanical cleavage, it possesses macroscopic (mm scale) lateral domains containing only microscopic (sub-micron scale) steps[21] and a high equilibrium contact angle (CA) for aqueous droplets (*ca.* 64° for water in air, with considerably higher values for aqueous solutions immersed in organic phases),[22,23] from which EWOC can be performed. We note that low-voltage EWOC on graphite has recently been reported,[24] although in this case, the process was dependent

a *School of Chemistry, University of Manchester, Oxford Road,*
 Manchester M13 9PL, UK. E-mail: robert.dryfe@manchester.ac.uk
b *MCND and School of Physics & Astronomy, University of Manchester,*
 Oxford Road, Manchester M13 9PL, UK

† Electronic supplementary information (ESI) available. See DOI: 10.1039/c6sm01565d
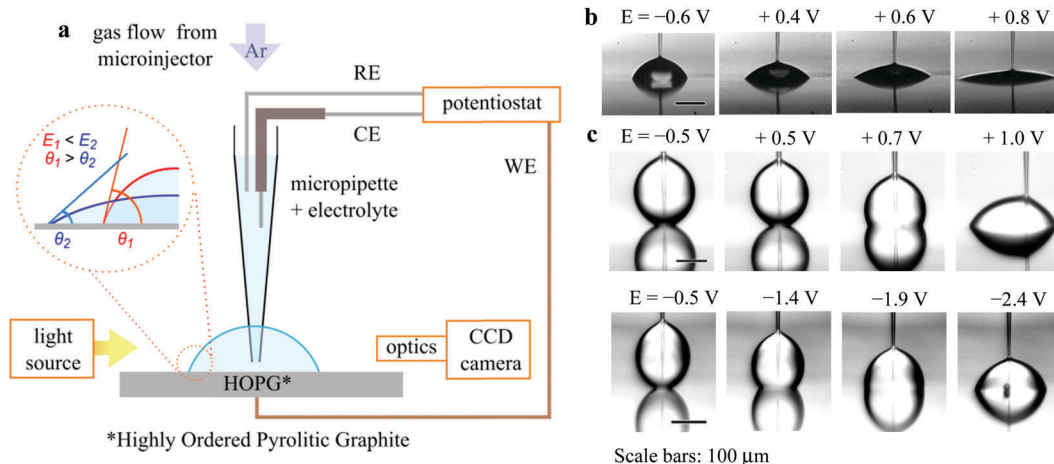
Fig. 1 (a) Schematic of the experiment: CE, RE and WE denote the counter, reference and working electrodes, respectively. CE is a Pt wire. (b) Images of an aqueous electrolyte droplet (6 M LiCl) in air of initial footprint diameter, d = 180 μm at different potentials $E = E_{WE} - E_{RE}$. The images show the droplet profile and its reflection on the HOPG substrate (see Experimental). (c) Images of aqueous electrolyte droplets (6 M LiCl) immersed in hexadecane with initial footprint diameter d = 51 μm (first row) and d = 77 μm (second row) at the potentials indicated.

on ion-intercalation, *i.e.* wetting involved graphitic edges (as opposed to the basal-plane), hence the notable contact angle hysteresis observed.

2. Experimental

Electrowetting was performed on HOPG (SPI–1 grade, from Structure Probe Inc., West Chester, PA, USA); the surface was renewed by cleavage with Scotch tape (3 M) immediately before each measurement. For liquid/air electrowetting, the HOPG was contacted on the reverse side using silver epoxy (RS Components Ltd) and Cu wire (0.25 mm diameter, 99.9%, Advent Research Materials, Witney, UK). For the liquid/liquid configuration, the same method was adapted using partially exposed PTFE-insulated Ag wire (0.20 mm wire diameter, 99.99%, Advent Research Materials) affixed with silver epoxy for the contact, masked by epoxy resin (Araldite).

A range of aqueous electrolyte solutions were prepared for liquid/air electrowetting: $\leq$6 M LiCl, 3 M MgCl$_2$, 3 M CsCl, 3 M LiOH, 3 M KOH, $\leq$3 M KF (all supplied by Sigma Aldrich) and 3 M KCl (Fluka). All solutions were made using ultrapure water (18.2 MΩ cm, "PURELAB" Ultrafiltration system, Elga Process Water).

Immiscible phases used in the liquid/liquid experiments were hexadecane (99%, Sigma Aldrich) or 1,2-dichlorobenzene (DCB, 99%, Aldrich). The latter was used to prepare organic electrolyte solutions of 0.02 M bis(triphenylphosphoranylidene)-ammonium tetrakis(4-chlorophenyl)borate (BTPPATPBCl). The synthesis of the BTPPATPBCl was adapted from the published procedure,[25] involving metathesis of bis(triphenylphosphoranyl-idene)ammonium chloride (Aldrich) and potassium tetrakis(4-chlorophenyl)borate (Sigma Aldrich) in 2 : 1 : 1 acetone : ethanol : water, followed by recrystallisation in 1 : 1 acetone : ethanol.[26]

Electrowetting was performed with an Autolab PGSTAT302N potentiostat (Metrohm Autolab, Utrecht, Netherlands) using a three electrode set-up, where the HOPG acted as the working electrode.

In the standard electrowetting configuration, droplets were deposited on the HOPG using a microinjector (PV820 Pneumatic PicoPump) to expel the electrolyte solution from a micropipette (drawn from borosilicate capillaries with a Sutter P-97 Flaming/Brown Micropipette Puller to give a tip with inner and outer diameters of approximately 0.5 microns and 2 microns, respectively). Where necessary to prevent evaporation, humid conditions were maintained by placing the HOPG within a glass cell containing a pool of ultra-pure water.

Both the HOPG and the micropipette were controlled using manual micro-positioners, so that the micropipette could be brought in close proximity to the surface and the smoothest regions of HOPG could be targeted. The micropipette also served as the electrolyte reservoir within which the auxiliary electrodes were located, $\approx$3 cm from the HOPG surface. These comprised of a Pt wire counter electrode (0.10 mm diameter, 99.99+%, Advent Research Materials) and a partially exposed polyester-insulated Pt wire pseudo-reference electrode (0.125 mm diameter, 99.99%, Goodfellow Cambridge Ltd, UK).

For the liquid/liquid configuration, the HOPG was immersed within the surrounding phase in a glass cell, followed by droplet placement with the microinjector. This configuration also allowed pipette-free electrowetting with application of the potential through the surrounding electrolyte phase, using a Pt mesh counter electrode (52 mesh per inch, 99.9%, Advent Research Materials) and Pt wire pseudo-reference electrode (0.3 mm diameter, 99.99%, Advent Research Materials).

The droplet shape during electrowetting was determined from side-on images primarily captured using a CCD camera (Infinity, Lumenera) with the droplet backlit using an LED light source. High speed imaging was performed at 10^4 frames per second (Fastcam SA3, Photron Ltd, Tokyo, Japan), coupled with a xenon light source (Xenon Nova 300, Karl Storz GmbH, Tuttlingen, Germany).

Contact angle values were extracted from the images using the gradient of the droplet edge near the contact line, following the

methodology of Neumann *et al.*[27,28] The images were processed with MATLAB™ (MathWorks Inc., Natick, MA, USA) to first perform background subtraction and then to find the droplet edge using the in-built Canny edge detection algorithm. The contact angle was extracted from the arcs representing the droplet edge near the contact line, implemented by fitting a 4th order polynomial to the Canny-determined edge. Calculation of θ then followed from the derivative of the polynomial at $z = 0$ where z is the distance from the surface, *i.e.* from the gradient at the surface:

$$\theta = \arctan\left(\frac{\mathrm{d}z}{\mathrm{d}x}\right) \qquad (1)$$

Macroscale electrochemistry was performed in the three electrode mode with the Pt wire pseudo-reference electrode (0.3 mm diameter, 99.99%, Advent) using the Autolab PGSTAT302N system. A Teflon cell (3 mm diameter aperture) was used to define the area of the freshly cleaved HOPG in contact with the electrolyte.

Electrical impedance spectroscopy (EIS) was performed with 6 M LiCl over a frequency range of $10-10^5$ Hz. The effective capacitance (C_{eff}) was determined using the method advocated by Tribollet *et al.* from graphical analysis for capacitance with a constant phase element contribution (when the exponent $\alpha \neq 1$).[29]

A value for α was calculated by performing a linear fit to a plot of the log of imaginary impedance (Z_j) (Ohm) *vs.* the log of frequency (f) (Hz):

$$\alpha = \left|\frac{\mathrm{d}\log|Z_j|}{\mathrm{d}\log f}\right| \qquad (2)$$

The effective capacitance (C_{eff}) was determined for each frequency using eqn (2), where:

$$C_{\mathrm{eff}} = \sin\left(\frac{\alpha\pi}{2}\right)\frac{-1}{Z_j(2\pi f)^\alpha} \qquad (3)$$

A range of C_{eff} values, determined by the linear portion of the C_{eff} *vs. f* plot, were then averaged to calculate the final capacitance, C, values.

The surface tension of the 6 M LiCl(aq.)/air interface was measured using an Attension Theta Lite Optical Tensiometer (Biolin Scientific AB, Stockholm, Sweden) with analysis performed with the corresponding OneAttension software: a value of 83.3 ± 0.1 mN m^{-1} was measured at 295 K.

Atomic force microscopy (AFM) was performed in PeakForce QNM tapping mode with a Multimode8 (Bruker) using silicon nitride SNL-10 cantilevers. Image analysis was performed with Nanoscope Analysis (v1.6, Bruker). All images were processed using the 2nd order "Flatten" procedure before analysis using the "Section" tool to determine step heights and the "Roughness" tool to find R_q and R_a, the root-mean-square (RMS) roughness and mean roughness, respectively, where z is the feature height and N is the number of measured features:

$$R_q = \sqrt{\frac{\sum Z_i^2}{N}} \qquad (4)$$

$$R_a = \frac{1}{N}\sum_{i=1}^{N}|Z_i| \qquad (5)$$

3. Results & discussion

3.1 Liquid/air EWOC

In the experimental setup shown in Fig. 1(a), a micropipette served both to place the droplet and to contain the electrolyte reservoir, within which the counter electrode (CE) and reference electrode (RE) were placed. The apparent CA of the droplet on HOPG was measured as a function of the potential applied to this substrate, E, with respect to a platinum pseudo-RE ($E = E_{\mathrm{WE}} - E_{\mathrm{RE}}$). Equilibrium sessile drops in air are presented in Fig. 1(b) as a function of E, showing the dramatic change in shape seen, using a range of E of only 1 V. Note that the potential of zero charge (pzc) of the 6 M LiCl system shown in Fig. 1 is $E_{\mathrm{pzc}} = -0.6$ V *vs.* the Pt pseudo-RE, for which the equilibrium CA is identical to the value with no applied bias ($\theta_{\mathrm{eq}} = 64 \pm 2°$). EWOC is not restricted to the case of an aqueous electrolyte surrounded by air: Fig. 1(c) shows the evolution of CA with E for an aqueous 6 M LiCl droplet immersed in hexadecane. Such concentrated solutions of aqueous LiCl have previously been employed for experiments in the EWOD configuration, to maximise the temperature range available.[6] The CA dependence, and associated diameter variations, on HOPG potential for the EWOC experiments are shown in Fig. 2(A) and (B) for the aqueous/air case (data presented in Fig. 1(b)): demonstrating reproducibility for droplets with initial footprint diameters (d) in the range 50 μm ≤ d ≤ 250 μm. The small biases applied are sufficient to induce electrowetting, but small enough to avoid electrolysis, see ESI,† Fig. S1. The low current densities associated with the EWOC mean that the power requirements are very low, on the order of 10 μW cm^{-2}.

Classical electrowetting theory describes the dependence of the cosine of θ on the applied potential, known as the Young–Lippmann equation:[12,13]

$$\cos\theta - \cos\theta_{\mathrm{eq}} = \gamma_{\mathrm{LV}}^{-1}\int_{E_{\mathrm{pzc}}}^{E} C(E)E\mathrm{d}E = \eta \qquad (6)$$

where $C(E)$ denotes the potential-dependent capacitance of the solid/liquid interface (HOPG/aqueous LiCl in this case), γ_{LV} is the surface tension between the two fluid phases (aqueous/air here), and η denotes the electrowetting number.[12]

A direct comparison of liquid/air EWOC with eqn (6) is presented in Fig. 2(C) by plotting the cosine of the CA data from Fig. 2(A) against η. Note that the interfacial capacitance is often treated as constant, using a Helmholtz model of the electrical double layer, where the only contribution to capacitance is ascribed to the layer of counter-ions adjacent to the surface. Whilst the resultant quadratic dependence on potential describes much of the extant EWOD data well, the approximation of constant capacitance is unrealistic for the EWOC case, due to the variation in electrode/electrolyte capacitance even over moderate excursions of potential.[30] The capacitance of such conductor/electrolyte interfaces is readily measured, with alternating voltage measurements of the frequency-dependent current response yielding the interfacial capacitance *via* the imaginary component of the total impedance. The capacitance is normally dominated by the solution side of the interface,[30] which can be decomposed into a Stern layer, consisting of ions specifically
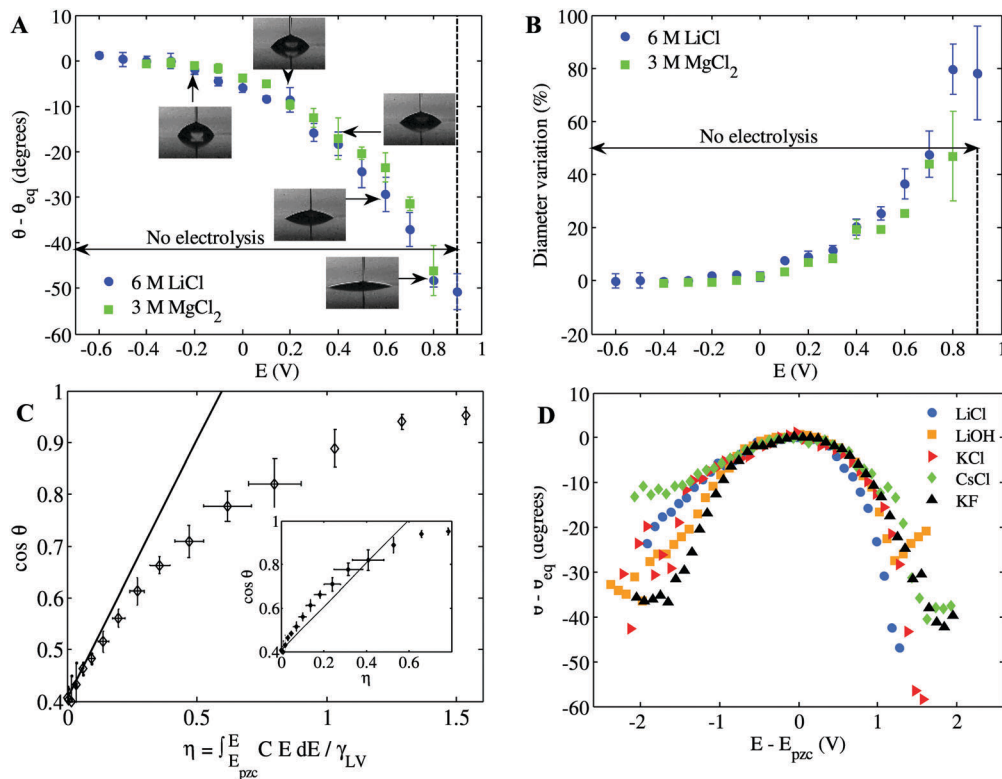
Fig. 2 (A) Change in apparent CA for $E \geq E_{pzc}$, showing averages and standard deviations of between 5 and 23 experiments. Solutions with equivalent chloride concentration show similar wetting. (B) Percentage change in the droplet footprint with E, including droplets with a fourfold variation in initial diameter. (C) Cosine of CA *versus* electrowetting number for the data presented in (A). Inset: same plot with potential correction for the space–charge region within the graphite in η. (see Experimental and ESI,† Fig. S2 for details of capacitance and surface tension measurements). (D) Effect of electrolyte identity on EWOC: the change in CA with potential (relative to the PZC of each electrolyte) for a variety of concentrated (3 M) aqueous electrolytes: LiCl, LiOH, KCl, CsCl and KF.

adsorbed on the surface (and dictated by the size of the constituent ions), and a diffuse double-layer component, however the latter term can be neglected at the higher electrolyte concentrations employed herein. $C(E)$ was accordingly measured *via* AC impedance (see ESI,† Fig. S2) and η was evaluated using the trapezoid rule at each value of E.

Fig. 2(C) shows that the measurements are consistent with the prediction of eqn (6) (solid line) at low bias. At higher biases, the observed CA change falls below the prediction based on the total capacitance, although the agreement is substantially improved if the potential is corrected for the space-charge region within the graphite (see inset of Fig. 2(C) and ESI,† Fig. S2).[31] The overall consistency between the calculated and experimental data implies that the EWOC phenomenon can be rationalized in terms of the capacitance of the electrical double-layer formed at the HOPG/droplet interface. This, in turn, highlights the role of the dielectric in inhibiting performance. Capacitance is inversely proportional to the thickness of the charged layer, this is up to several microns thick for a typical dielectric in EWOD,[32] compared with an electrical double layer in the high electrolyte EWOC configuration on the order of 1 nm.[30] Hence eqn (6) implies that a 100-fold increase in potential (given the approximate square dependence) is required for EWOD to compensate for the 10^4-fold decrease in capacitance associated with the presence of the dielectric.

The EWOC phenomenon on graphite is robust, being observed for a range of aqueous electrolytes, from molar to sub-millimolar concentrations, see Fig. 2(D) and ESI,† Fig. S3. The subtle differences between electrolytes are attributed to specific ion-graphite surface interactions, manifested as asymmetry of the CA dependence with respect to E_{pzc}, and shifts in the value of E_{pzc}. To correct for the effect of the latter, the data in Fig. 2(D) is plotted relative to E_{pzc} for each electrolyte (see Table S1 of ESI†). Overall, the data of Fig. 2 reveals another key property of HOPG surfaces that is essential to their function in EWOC, namely the low electrochemical activity of the HOPG basal plane, particularly for electrolytic processes requiring a catalytic function.[21] Metallic surfaces are much more susceptible to the formation of surface oxides and/or electrocatalytic processes associated with water decomposition, which reduce the zone of stability of metal/solution interfaces with respect to electrolysis.[10,30] The lower activity of graphite, coupled with its layered (hence smooth, see ESI,† Fig. S4) structure explains why hysteresis-free wetting can be achieved at low voltages without solution electrolysis, as the current–voltage data (ESI,† Fig. S1 and S5) shows. ESI,† Fig. S4 also presents an analysis of the influence of the height of steps within the HOPG basal plane on the wetting response: steps larger than *ca.* 100 nm appear to pin the droplets. For the grade of HOPG used, domains of 10–100 microns exist

with steps below this threshold height, hence this range of droplet sizes was employed for the wetting experiments.

3.2 Liquid/liquid EWOC

Extension of the EWOC phenomenon to liquid/liquid configurations on HOPG, is also demonstrated, see Fig. 1(c). The CA and diameter variations for 6 M LiCl droplets in hexadecane are shown in Fig. 3(A) and (B). Electrowetting is seen at both positive and negative potentials (with respect to $E_{pzc} = -0.5$ V) although the potential dependence is more complex than the liquid/air case. In the liquid/liquid case, potential thresholds must be overcome to induce wetting, as no CA change is observed over a potential range around E_{pzc} (see Fig. 3(A), diameter changes are shown in Fig. 3(B)). A 60° change occurs in the range -1 V > E > -2 V: electrowetting continues at more negative potentials, electrolysis also begins with gas formation clearly evident at –2.4 V. By contrast the positive wetting branch does not suffer from electrolysis, is hysteresis-free (ESI,† Fig. S5 and S6), and offers better performance giving a CA range of 100° over 1.5 V. The flexibility of EWOC on HOPG is demonstrated in Fig. 3(C–E) and ESI,† Fig. S7. Electrowetting with the EWOD configuration can be achieved with immiscible liquid phases:[6] one containing electrolyte, which spreads on application of $E \neq E_{pzc}$, and an immiscible ion-free phase. A variation on this approach, proposed by Kornyshev et al. for the EWOC configuration on gold,[11,14–17] achieves such pipet-free electrowetting with ions present in both liquid phases. The latter approach is replicated here on HOPG and substantial changes in CA are seen, consistent

with the changes predicted for this configuration,[11] which are repeatable over a number of cycles: again, because of the absence of pinning, pulsing of the potential is not required.

The ability to perform EWOC in both liquid/air and immiscible liquid configurations should provide new insight into the outstanding question of CA saturation with potential in EWOD, which is frequently seen at $\theta \geq 45°$.[12,32] CAs as low as 10° are reached in the liquid/air configuration with only minimal evidence of CA saturation (Fig. 2), whereas saturation is seen at $\theta \simeq 47°$ in the liquid/liquid configuration (Fig. 3). The higher voltages required for liquid/liquid EWOC (supported by the wider potential range before electrolysis, see ESI,† Fig. S3(f)) are consistent with the presence of an ultra-thin layer of organic liquid between the droplet and the substrate,[33,34] likening this configuration to EWOD, albeit at ultra-low voltages. This suggests that CA saturation may be associated with the presence of a dielectric layer, therefore supporting dielectric breakdown as underlying saturation.[35,36]

Much of the interest in the phenomenon of electrowetting stems from its applications,[2,6,8] for which reproducibility and the timescale of CA response are critical. Fig. 4(A) shows that highly reproducible changes (to within 1% over 450 cycles) of CA and droplet diameter are obtained for the liquid/air case. Moreover, pronounced CA hysteresis between spreading and de-wetting cycles has been observed in prior approaches to EWOD[12,13] and EWOC[16] whilst here we find a remarkably low hysteresis of <2° for $E \leq 0.7$ V, Fig. 4(B–D). Increased hysteresis (up to 7°) is seen when E is extended to 0.8 V, due to droplet
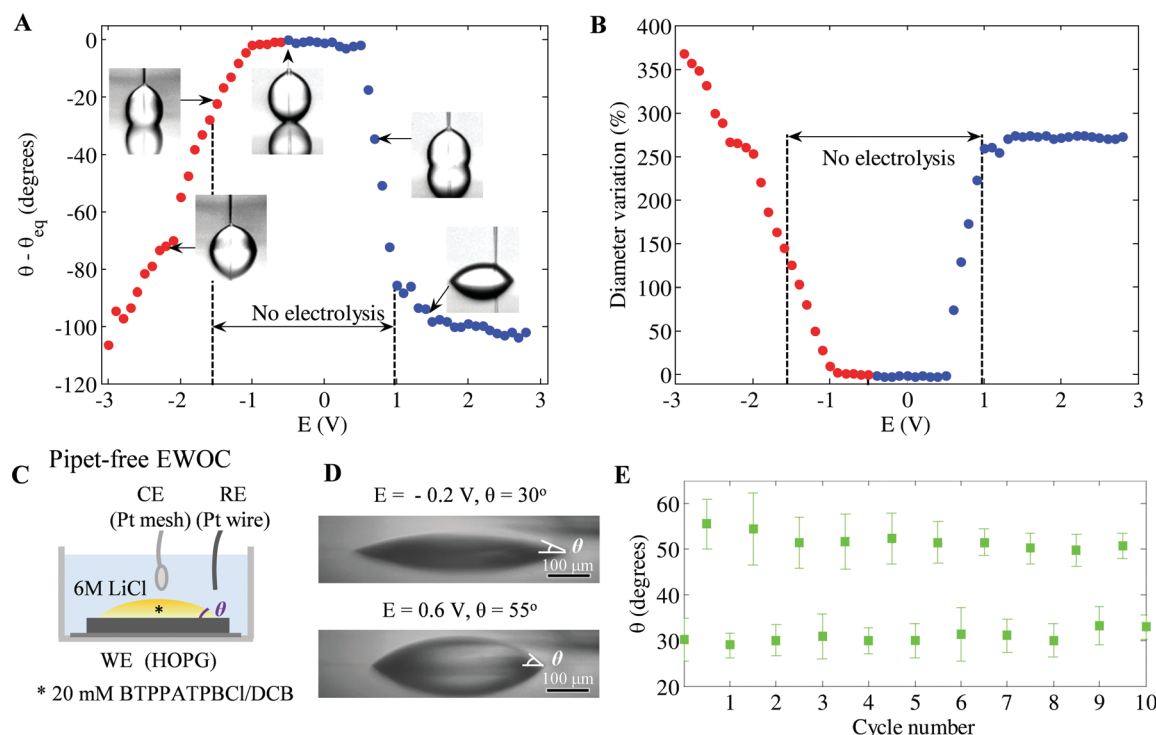
Fig. 3 (A) Change in CA as a function of E in steps of ±0.1 V. Blue and red symbols indicate $E > E_{pzc}$ and $E < E_{pzc}$, respectively. Changes in CA of up to 90° below the electrolysis threshold for $E > E_{pzc}$ are followed by saturation, see ESI† for electrolysis data. For $E < E_{pzc}$, CA decreases monotonically. (B) Percentage change in the footprint diameter of the droplet with E. (C) Pipette-free configuration used to illustrate generality of liquid/liquid EWOC, (D) change in CA with E, and (E) cycling data for steps in E between −0.2 V and +0.6 V (right).
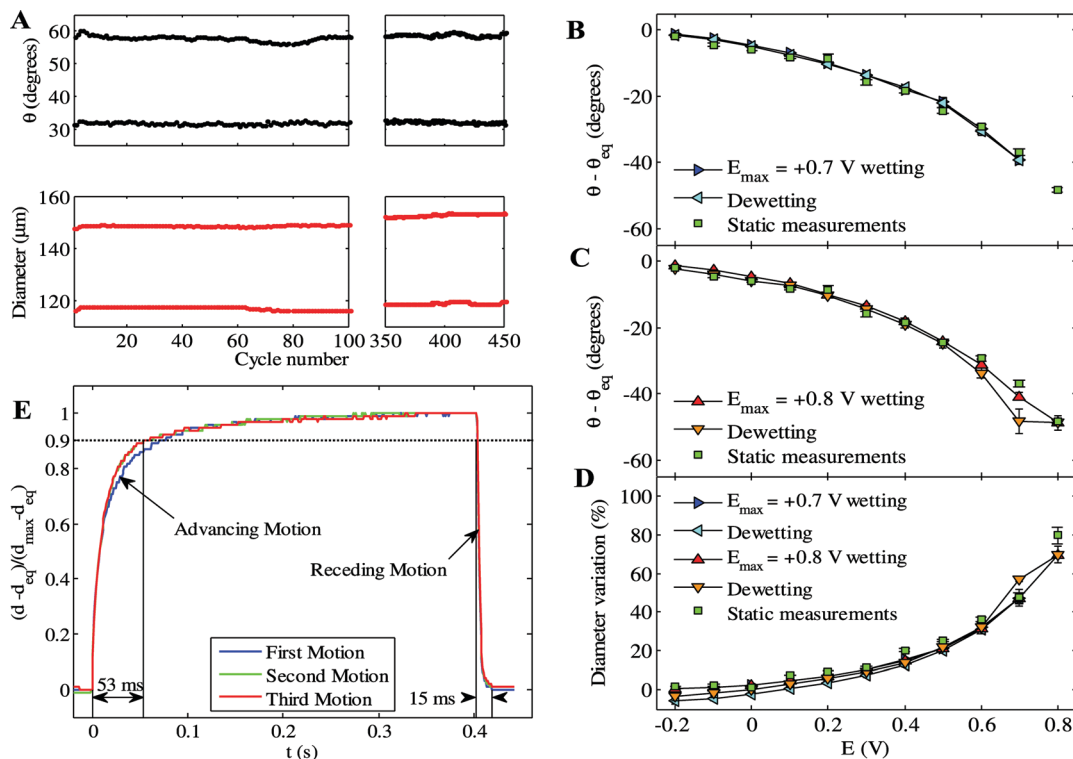
Fig. 4 (A) Constant CA and drop diameter of aqueous 6 M LiCl in air (to within ±1%) over 450 cycles of potential steps between $E = -0.2$ V and +0.6 V, step duration = 0.25 s. (B) Comparison between CA on stepping E from an initial $E = -0.2$ V (static measurements, see Fig. 2), and incrementing between -0.2 V and +0.7 V in 0.1 V steps (wetting), then -0.1 V (de-wetting). (C) Same as in b with E incremented to +0.8 V. (D) Same comparison of diameter variation. (E) Change in footprint diameter (from 290 μm to 219 μm) with time over three cycles of step-change from $E = -0.2$ V to +0.7 V.

pinning at the associated low CA (see Fig. 4(B)), although the low-hysteresis response is recovered when E is lowered to 0.5 V.

3.3 Dynamics of EWOC

The dynamics of the electrowetting process, and indeed surface wetting more generally, is an area of debate in current literature.[12,13,32] The dynamics of EWOC are shown in Fig. 4(E), which reveals that the CA adjusts on a timescale of 0.01 s. The intrinsic smoothness of the HOPG substrate[21] facilitates the lateral motion of the droplet (see ESI,† Fig. S4), reflected as minimal difference between the initial and subsequent cycles, with an asymmetry seen in the timescales of advancing and receding droplet motion.

4. Conclusion

We conclude by emphasizing the unique properties of laminar materials such as basal plane HOPG – smoothness and low intrinsic electroactivity – which, in combination with the high initial contact angle inherent to aqueous electrolytes, allow for the demonstration of hysteresis-free CA control via electrowetting on a solid conductor. The absence of a dielectric film maximizes the electrowetting effect by increasing the capacitance, an effect further amplified at high electrolyte concentrations, thus magnifying the dependence of the potential-dependent term in the Young–Lippmann equation. The process is shown to be rapid, reproducible and stable, with a voltage requirement at least one order of

magnitude lower than that typically required by current EWOD configurations. The removal of the dielectric layer, and the better defined nature of the HOPG/electrolyte interface, allows outstanding questions concerning the role of specific molecular interactions in controlling the electrowetting process to be addressed.

Note added after first publication

This article replaces the version published on the 30th of September 2016, which contained errors in the Fig. 2 caption.

Data statement

The data files relating to this work can be found at: http://www.mub.eps.manchester.ac.uk/robert-dryfe-electrochemistry/.

Competing financial interests

A patent application relating to this material has been filed by the University of Manchester.

Acknowledgements

References

1 *Micro and nanoscale phenomena in tribology*, ed. Y.-W. Chung, CRC Press, 2012.

2 A. R. Wheeler, *Science*, 2008, **322**, 539.

3 N. J. Cira, A. Benusiglio and M. Prakash, *Nature*, 2015, **519**, 446.

4 F. Mugele and J.-C. Baret, *J. Phys.: Condens. Matter*, 2005, **17**, R705.

5 B. Berge, *C. R. Acad. Sci., Ser. II: Mec., Phys., Chim., Sci. Terre Univers*, 1993, **317**, 157.

6 S. Kuiper and B. H. W. Hendriks, *Appl. Phys. Lett.*, 2004, **85**, 1128.

7 R. Shamai, D. Andelman, B. Berge and R. Hayes, *Soft Matter*, 2008, **4**, 38.

8 M. G. Pollack, A. D. Shenderov and R. B. Fair, *Lab Chip*, 2002, **2**, 96–101.

9 G. Lippmann, *Ann. Chim. Phys.*, 1875, **5**, 494–549.

10 A. Frumkin, A. Gorodetzkaja, B. Kabanow and N. Nekrassow, *Phys. Z. Sowjetunion*, 1933, **1**, 255.

11 C. W. Monroe, L. I. Daikhin, M. Urbakh and A. A. Kornyshev, *Phys. Rev. Lett.*, 2006, **97**, 136102.

12 F. Mugele, *Soft Matter*, 2009, **5**, 3377–3384.

13 R. Sedev, *Eur. Phys. J.: Spec. Top.*, 2011, **197**, 307.

14 C. W. Monroe, M. Urbakh and A. A. Kornyshev, *J. Phys.: Condens. Matter*, 2007, **19**, 375113.

15 C. W. Monroe, M. Urbakh and A. A. Kornyshev, *J. Electrochem. Soc.*, 2009, **156**, P21.

16 A. A. Kornyshev, *et al.*, *J. Phys. Chem. C*, 2010, **114**, 14885.

17 M. Marinescu, T. Barnea, M. Urbakh and A. A. Kornyshev, *J. Phys. Chem. C*, 2010, **114**, 22558.

18 F. Li and F. Mugele, *Appl. Phys. Lett.*, 2008, **92**, 244108.

19 D. J. C. M. 't Mannetje, C. U. Murade, D. van dan Ende and F. Mugele, *Appl. Phys. Lett.*, 2011, **98**, 014102.

20 M. Maillard, J. Legrand and B. Berge, *Langmuir*, 2009, **25**, 6162.

21 R. L. McCreery, *Chem. Rev.*, 2008, **108**, 2646.

22 Z. Li, *et al.*, *Nat. Mater.*, 2013, **12**, 925.

23 C. A. Amadei, C. Y. Lai, D. Heskes and M. Chiesa, *J. Chem. Phys.*, 2014, **141**, 084709.

24 G. Zhang, M. Walker and P. R. Unwin, *Langmuir*, 2016, **32**, 7476.

25 F. Reymond, *et al.*, *J. Electroanal. Chem.*, 1999, **462**, 235.

26 A. N. J. Rodgers, M. Velický and R. A. W. Dryfe, *Langmuir*, 2015, **31**, 13068.

27 O. I. Del Río, D. Y. Kwok, R. Wu, J. M. Alvarez and A. W. Neumann, *Colloids Surf., A*, 1998, **143**, 197.

28 A. Bateni, S. S. Susnar, A. Amirfazli and A. W. Neumann, *Colloids Surf., A*, 2003, **219**, 215.

29 M. E. Orazem, N. Pébère and B. Tribollet, *J. Electrochem. Soc.*, 2006, **153**, B129.

30 H. H. Girault, *Analytical and Physical Electrochemistry*, EPFL Press-John Wiley, 2004.

31 H. Gerischer, *J. Phys. Chem.*, 1985, **89**, 4249.

32 M. Paneru, C. Priest, R. Sedev and J. Ralston, *J. Am. Chem. Soc.*, 2010, **132**, 8301.

33 C. Shi and F. C. Anson, *Anal. Chem.*, 1998, **70**, 3114.

34 C. Quilliet and B. Berge, *Europhys. Lett.*, 2002, **60**, 99.

35 A. I. Drygiannakis, A. G. Papathanasiou and A. G. Boudouvis, *Langmuir*, 2009, **25**, 147.

36 M. Vallet, M. Vallade and B. Berge, *Eur. Phys. J. B*, 1999, **11**, 583.